

All-electron full-potential calculation of the electronic band structure, elastic constants, and equation of state for graphite

J. C. Boettger

Theoretical Division, Los Alamos National Laboratory, Los Alamos, New Mexico 87545

(Received 15 November 1996)

The all-electron full-potential linear combinations of Gaussian-type orbitals—fitting-function technique has been used to calculate the electronic structure, equation of state (EOS), and elastic constants for crystalline graphite. An analysis of the zero-pressure band structure is used to resolve inconsistencies between previous local-density-approximation (LDA) calculations. The calculated band structure is consistent with experimental data to the extent expected given the known limits of LDA one-electron energies. The in-plane lattice constant found here exhibits the usual LDA-induced contraction, whereas the interlayer separation and the unit-cell volume exhibit an anomalous expansion due to a LDA underestimate of the weak interlayer bonding. The calculated values of $C_{11} + C_{12}$ and C_{33} are in good agreement with ultrasound measurements, while the value of C_{13} (≈ 0) is much smaller than the ultrasound value. The bulk modulus and pressure derivatives of the lattice constants derived from the theoretical elastic constants are in very good agreement with diamond anvil cell (DAC) data, suggesting that the theoretical value for C_{13} is more reliable than the ultrasound measurement. An analytical EOS has been determined for pressures up to 50 GPa, well beyond the range of stability for the graphite structure. The EOS and the pressure dependencies of c/a and the optical transition energies (A_1 and A_2) are in reasonable agreement with DAC data up to 14 GPa. [S0163-1829(97)01118-1]

I. INTRODUCTION

Graphite is a prototypical layered material, characterized by exceptionally strong sp^2 covalent intralayer bonding and weak van der Waals interlayer bonding. This highly anisotropic bonding gives rise to a number of unusual properties that are of long-standing technological and scientific importance.¹ Over the last two decades, there has been a resurgence of interest in graphite as a primary component of the graphite intercalation compounds formed by inserting various atoms or molecules between the loosely bonded layers of a graphite crystal.² For these reasons, a wealth of experimental data has been amassed relating to the equation of state (EOS),³⁻⁷ elastic constants,^{4,8-12} and energy bands^{6,13-33} of graphite. Graphite also was one of the earlier materials studied with electronic structure techniques¹ and has been the subject of numerous theoretical investigations over the years.³⁴⁻⁴⁵

In spite of all this activity, the theoretical picture of graphite remains incomplete. The local-density-approximation (LDA) electron energy band calculations for bulk graphite carried out over the last decade have included three pseudopotential (PP) calculations^{41,43,44} and two all-electron calculations; one using the full-potential linearized augmented plane-wave (FLAPW) method⁴⁰ and the other using the full-potential linear muffin-tin-orbital (FLMTO) method.⁴⁵ Although the various band-structure calculations are in good qualitative agreement, there are large quantitative differences between them. In particular, the band energies determined with the two all-electron methods differ by as much as 1.9 eV; a rather disturbing result given that these techniques are routinely applied to systems with unit cells containing hundreds of electrons, versus 24 for graphite. Few electronic structure calculations to date have addressed the

high-pressure EOS (Refs. 39, 40, and 44) and elastic constants⁴⁰ of graphite.

In the present investigation, the all-electron, full-potential linear combinations of Gaussian-type orbitals fitting-function (LCGTO-FF) technique has been used to calculate the electronic band structure and total energy of graphite in the Bernal structure⁴⁶ (i.e., with AB stacking) for various combinations of the hexagonal lattice parameters a and c . The total energies have been used to determine the lattice parameters, elastic constants, and EOS for graphite. In the next section, the basis sets used and other details of the calculations will be discussed briefly. In Sec. III, the calculated band structure for graphite near the equilibrium geometry will be assessed for numerical stability and will be compared with previous theoretical results in an attempt to resolve some of the discrepancies in the literature. Results for the zero-pressure geometry and elastic constants will be presented in Sec. IV. The EOS and high-pressure properties will be discussed in Sec. V. A few concluding remarks will be given in the final section.

II. TECHNICAL DETAILS

The calculations reported here employed the all-electron, full-potential LCGTO-FF electronic structure technique as embodied in the program package GTOFF,⁴⁷ a generalization of the two-dimensional (2D) electronic structure program FILMS (Refs. 48 and 49) to include 3D periodicity. The LCGTO-FF technique is distinguished from other extant electronic structure methods by its use of three independent GTO basis sets to expand the orbitals, charge density, and LDA exchange-correlation (XC) integral kernels; here using the LDA parametrization of Hedin and Lundqvist (HL).⁵⁰ The charge-fitting functions are used to reduce the total number of Coulomb integrals by replacing the usual four-center

integrals in the total energy and one-electron equations with three-center integrals. The charge-fitting function coefficients are determined by minimizing the error in the Coulomb energy due to the fit,⁵¹ thereby allowing high-precision calculations with relatively small basis sets.⁵² (This use of variational charge fitting clearly distinguishes the LCGTO-FF method from earlier fitting-function-based methods,^{53–55} in which the charge density and/or the potential were least-squares fitted.) The least-squares XC fit used here acts as a simple yet sophisticated numerical quadrature scheme capable of producing accurate results with a rather coarse numerical integration mesh. The overall precision of any LCGTO-FF calculation will, of course, be largely determined by the selection of these three basis sets.

Several distinct orbital and fitting-function basis sets were used during the course of this investigation, both to test the numerical stability of the calculations and to tailor the basis sets used in a given portion of the investigation to the range of lattice parameters under consideration. All of the orbital basis sets used here were derived from a single reference basis set; a $12s6p1d$ primitive GTO basis set contracted into a $7s3p1d$ basis set and augmented with a single diffuse p_z -type GTO to better describe the strong anisotropy in the bonding. Reference basis sets also were developed for the fitting functions; an $8s2d$ charge basis and a $7s2d$ XC basis. All three of these reference basis sets have been described in detail elsewhere.⁵⁶ Modifications made in the reference basis sets will be described as needed.

All necessary Brillouin-zone (BZ) integrations were carried out via the linear tetrahedral method⁵⁷ on a uniform $12 \times 12 \times 6$ mesh with 76 irreducible k points. During each calculation, the self-consistent field (SCF) cycle was iterated until the total energy changed by less than $1 \mu\text{Ry}$ per atom.

III. EQUILIBRIUM BAND STRUCTURE

The band structure of crystalline graphite is closely related to that of graphene; a monolayer extracted from graphite. In fact, many early band-structure calculations used graphene as a model for graphite.³⁴ The electron orbitals in graphene are classified as σ (π) states if they have even (odd) symmetry under reflection through the atomic plane. The band structure of graphene near the Fermi level is comprised of three occupied σ bands derived from the $2s$, $2p_x$, and $2p_y$ atomic states, a pair of π bands derived from the $2p_z$ atomic states (one nearly full and the other nearly empty), and a series of unoccupied bands. Since each unit cell of graphite contains two very weakly bonded unit cells of graphene, the band structure of graphite can be roughly approximated by splitting each graphene band into two, with the splitting being largest at the bottom of each band. These features are illustrated in Fig. 1, which shows the energy bands obtained here for graphite with $a=4.651$ bohr and $c/a=2.75$, using the reference basis sets described earlier.

Table I lists the energies obtained here for the states at the Γ point and the splittings of the π bands at the K point (using the notation of Ref. 58), and compares them with results from other LDA calculations.^{40,41,43–45} As was noted earlier, there are significant quantitative differences between the various calculations. Since all of the calculations listed in Table I used either the HL LDA model or the

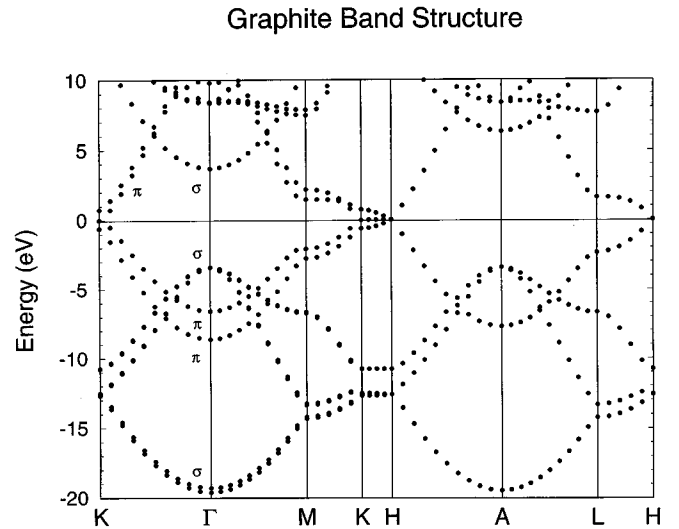


FIG. 1. The electronic band structure obtained here for graphite using the reference basis sets. The zero of energy is the Fermi energy. All energies are in eV.

Perdew-Zunger⁵⁹ (PZ) LDA model, a LCGTO-FF calculation was carried out using the PZ model to test for sensitivity to the LDA model chosen. The PZ results differed from the HL results by no more than 0.01 eV. Thus, the differences between the calculations must be due to computational imprecision.

If the first six calculations listed in Table I are taken as a whole, it is possible to identify several quantitative features of the band structure of graphite for which at least five of the six calculations agree. (1) The bottom of the occupied σ band is located roughly 20 eV below the Fermi level and is split by about 0.3 eV. (2) The bottom of the π band is located about 9 eV below the Fermi level and is split by 2 eV. (3) The top of the occupied σ band is slightly more than 3 eV below the Fermi level and is split by no more than 0.1 eV. (4) The first unoccupied σ band is slightly less than 4 eV above the Fermi level. If these features are taken to represent the “correct” LDA band structure for graphite, it is then possible to identify “errors” in both of the previous all-electron calculations.

The FLAPW calculation⁴⁰ places the top of the occupied σ band roughly 1 eV lower than any other calculation. In Ref. 40, it was noted that the energy of that state was sensitive to the number of k points used for the BZ integrations. In contrast, Schabel and Martins⁴³ found that the energy of that state is rapidly convergent with the number of k points used, varying by only 3 meV when they increased the number of irreducible k points from 6 to 40, and concluded that the discrepancy between the FLAPW and PP results was due to differences in the BZ sampling schemes employed. During this investigation, it was found that increasing the number of irreducible k points from 76 to 185 changed the band energies by no more than 0.03 eV, in general agreement with Schabel and Martins.⁴³ Given the fact that the FLAPW calculations used 140 irreducible k points (more than 20 times as many as the smallest set considered by Schabel and Martins), it is difficult to imagine that any reasonable method for selecting those 140 k points could produce a 1 eV lowering

TABLE I. Energies of the σ and π states at the Γ point relative to the Fermi energy and the splittings of the π bands at the K point from various calculations; all energies are in eV. The notation used here is consistent with Ref. 58. (a) Charlier *et al.* (Ref. 41), PP; (b) Schabel and Martins (Ref. 43), PP; (c) Furthmüller *et al.* (Ref. 44), PP; (d) Jansen and Freeman (Ref. 40), FLAPW; (e) Ahuja *et al.* (Ref. 45), FLMTO with a $2s2p2d$ basis; (f) present work, LCGTO-FF with reference basis sets; (g) present work, LCGTO-FF with an enriched d fitting function basis; (h) Wills (Ref. 60), FLMTO with an enriched $5s5p2d2f$ basis.

State	Pseudopotential			All electron			Enriched	
	<i>a</i>	<i>b</i>	<i>c</i>	<i>d</i>	<i>e</i>	<i>f</i>	<i>g</i>	<i>h</i>
σ	-20.1	-19.6	-19.7	-19.6	-19.2	-19.61	-19.54	-19.66
	-19.8	-19.2	-19.35	-19.3	-19.2	-19.31	-19.24	-19.38
π	-8.9	-8.7	-8.8	-8.7	-7.8	-8.62	-8.59	-8.46
	-6.8	-6.6	-6.7	-6.7	-6.4	-6.59	-6.61	-6.54
σ	-3.5	-3.0	-3.05	-4.6	-3.4	-3.41	-3.28	-3.25
	-3.4	-3.0	-3.0	-4.6	-3.4	-3.40	-3.26	-3.24
σ	3.7	3.9	3.8	3.8	5.7	3.68	3.94	4.55
	7.9	8.4	8.5	8.3	7.9	8.34	8.41	8.17
	7.9	8.4	8.5	8.4	8.0	8.38	8.46	8.22
$E_3 - E_2$	0.80	0.58			0.57	0.61	0.60	
$E_1 - E_3$	0.86	0.74			0.68	0.74	0.73	

of the highest occupied σ band relative to the other bands. It seems more likely that the FLAPW calculation suffered from some form of basis set induced numerical instability in the p_x and p_y states near the Γ point.

The FLMTO calculation⁴⁵ disagrees with all of the other calculations listed in Table I with regards to several of the basic features of the band structure for graphite. First, the FLMTO calculation found no splitting at the bottom of the occupied σ band. In fact, one of the conclusions of Ahuja *et al.*⁴⁵ was that the degeneracy of the σ bands could be removed by reducing the volume under pressure. The FLMTO calculation also significantly underestimated the splitting at the bottom of the π -band; finding a 1.4-eV splitting versus the roughly 2-eV splitting found in all of the other calculations. Finally, the FLMTO calculation places the lowest unoccupied σ state nearly 2 eV further above the Fermi level than any other calculation. None of these large discrepancies with the existing literature was remarked upon in Ref. 45. Since the σ and π band splittings are closely related to the interplanar bonding and the first unoccupied σ state extends far into the interplanar region, the discrepancies are most likely related to the selection of the tail parameters used in the FLMTO calculation.

The three PP calculations are all in reasonable agreement with the present LCGTO-FF calculation. The remaining discrepancies can be attributed to differences in basis set richness and variations in the pseudopotentials used in the three older calculations. To pin down the locations of the bands more precisely, several LCGTO-FF calculations were carried out using enriched basis sets. First, the orbital basis was increased to an $8s5p2d$ contracted basis set augmented with one additional p_z GTO. The resulting band energies differed from the values in column *f* of Table I by only a few hundredths of an eV, indicating good convergence of the band energies with respect to the orbital basis set size. Calculations were then carried out using the reference orbital basis set with various enriched fitting function basis sets. The ‘‘best’’ fit, as measured by test parameters calculated in

GTOFF, was achieved with charge and XC basis sets in which the two d -type fitting functions of the reference basis sets were replaced by three; see column *g* of Table I. Only two significant changes occurred in the band structure: (1) all of the σ bands were shifted upward relative to the π bands by about 0.1 eV; (2) the first unoccupied σ band is shifted up relative to the other σ bands by another 0.2 eV. These shifts provide a rough estimate for the uncertainty in the present results.

To clarify matters with regards to the FLMTO calculation, one of the authors of Ref. 45, Wills, has performed FLMTO calculations on graphite using basis sets of various sizes with optimized tail parameters.⁶⁰ The smallest basis set employed was the same size as that used in Ref. 45 ($2s2p2d$); an example of the so-called ‘‘double-basis sets’’ that are commonly used for high accuracy FLMTO calculations. Although the use of optimized tail parameters increases the σ and π band splittings, the double-basis set calculation still underestimates both splittings by about 20%. When the FLMTO basis set size is increased, the occupied band energies converge rapidly to values that are in good agreement with the values found here. The band energies obtained with the largest optimized FLMTO basis set ($5s5p2d2f$) are listed in column *h* of Table I. (Note that this enriched FLMTO basis set is larger than the double-basis sets that were used to study the electronic structures and phase stabilities of three light actinide metals.⁶¹) The enriched basis-set FLMTO and LCGTO-FF results for graphite agree to within about 0.15 eV for all of the occupied band energies. However, the enriched basis-set FLMTO calculation still places the unoccupied σ band about 0.6 eV too high relative to the Fermi level. This result may reflect the fact that a basis set which has been optimized by minimizing the total energy may not provide the best possible representation for the unoccupied states.

The ‘‘best’’ fit results obtained here (column *g* of Table I) are compared with experimental band energies from various sources in Table II. The occupied band structure of graphite

TABLE II. The best fit LCGTO-FF LDA results for the energies of the σ and π states at the Γ point relative to the Fermi energy and the splittings of the π bands at the K point are compared with experimental values; all energies are in eV. (a) Eberhardt *et al.* (Ref. 18); (b) Law *et al.* (Ref. 22); (c) Marchand *et al.* (Ref. 23); (d) Takahashi *et al.* (Ref. 24); (e) Hanfland *et al.* (Ref. 6); (f) Bellodi *et al.* (Ref. 14); (g) Fauster *et al.* (Ref. 21), Schäfer *et al.* (Ref. 28), Maeda *et al.* (Ref. 29), Claessen, *et al.* (Ref. 31), and Collins *et al.* (Ref. 32).

State	LDA	ARPES				IR		ARIPES
		<i>a</i>	<i>b</i>	<i>c</i>	<i>d</i>	<i>e</i>	<i>f</i>	<i>g</i>
σ	-19.54 -19.24	-20.6						
π	-8.59 -6.61	-8.1 -7.2	-8.5 -6.5	-9.0 -7.6	-9.3 -8.1			
σ	-3.28 -3.26	-4.6 -4.6	-5.5 -5.5	-5.3 -5.3	-4.3 -4.3			
σ	3.94 8.41 8.46							4.5–5.0 9.5–10.0 9.5–10.0
$E_3 - E_2$	0.60					0.68	0.74	
$E_1 - E_3$	0.73					0.81	0.88	

has been studied extensively over the years^{1,16–18,22–24} using a wide variety of techniques, including angle-resolved photoemission spectroscopy (ARPES). Columns *a–d* in Table II list energies obtained from ARPES measurements^{18,22–24} for the occupied states at the Γ point. Although there is considerable scatter in the data, presumably due to difficulties in resolving the individual features of the spectra, there does not appear to be any disagreement about the assignments of those peaks to particular critical points in the band structure. The π band splittings at the K point have also been identified unambiguously in the infrared reflectance (IR) spectra of graphite. Results from two IR measurements^{6,14} are listed in columns *e* and *f* of Table II.

The unoccupied band structure of graphite was the subject of theoretical and experimental controversy for several years. The focus of that controversy was the location of the lowest unoccupied σ band, which is associated with a state that is localized in the interlayer region, as is evidenced by its rather large (2.9 eV) dispersion in the *c* direction between the Γ and *A* points; see Fig. 1. Angle-resolved inverse photoemission spectroscopy (ARIPES) measurements by Fauster *et al.*²¹ in 1983 located the bottom of this “interlayer” band 4.0 ± 0.5 eV above the Fermi level, in good agreement with a PP calculation by Holzwarth *et al.*³⁶ Later that same year, angle-resolved secondary electron emission spectroscopy (ARSEES) measurements by Law *et al.*²² suggested that the bottom of the unoccupied σ band actually was located 7.6 eV above the Fermi level, in good agreement with a second PP calculation by Tatar and Rabii.³⁴ Subsequent ARIPES measurements^{27–29,31,32} consistently located the “interlayer” band 4.5–5.0 eV above the Fermi level, whereas all other measurements^{23,25,26,29} placed it about 7.5 eV above the Fermi level. In 1988, Maeda *et al.*²⁹ persuasively argued, on the basis of an analysis of ARIPES and ARSEES measurements, that only the former technique was able to discern the bottom of the unoccupied σ band, and that the structure being seen at 7.5 eV with the other methods was actually associated with an unoccupied state at the *A* point. The range of conduction band energies found in several ARIPES experiments^{21,28,29,31,32} are listed in column *g* of Table II.

Comparison of the “best” fit LDA results for the band

energies and splittings of graphite with the experimental values in Table II reveals several interesting features: (1) The LDA energies for the occupied π bands fall within the range of the ARPES data; (2) the LDA energies for the occupied σ bands are consistently higher than the ARPES data by at least 1 eV; (3) the LDA values for the splittings in the π bands near the K point are in good agreement with the IR data, albeit slightly smaller; and (4) the LDA energies for the unoccupied σ bands are smaller than the values taken from the ARIPES measurements by 0.7–1.6 eV. These features can all be understood in terms of the known limitations of the LDA. In general, LDA calculations tend to underestimate separations between energy bands; the well-known band gap problem. Since the Fermi level is pinned at the junction of the bonding and antibonding π bands, the LDA energies for those bands relative to the Fermi level are in reasonably good agreement with the experimental data. The occupied (unoccupied) σ bands are then shifted upwards (downwards) relative to the π bands and the pinned Fermi level, by roughly 1 eV. Thus, the LDA energies listed in Table II provide a theoretical picture for the electronic structure of graphite that is consistent with the available data.

IV. LATTICE PARAMETERS AND ELASTIC CONSTANTS

The reference basis sets were used to calculate the binding energies (E_b) of graphite for 24 distinct combinations of the hexagonal lattice parameters *a* and *c*, with *a* ranging from 4.5 to 4.7 bohr and *c/a* ranging between 2.5 and 3.0. The low-pressure properties of graphite were then determined by least-squares fitting the calculated binding energies with a generalized two-dimensional cubic function of *a* and *c* with the form

$$E(a, c) = \sum_{i=0}^3 \sum_{j=0}^{3-i} D_{ij} (a - a_0)^i (c - c_0)^j, \quad (1)$$

where a_0 and c_0 are the values of *a* and *c* at the local energy minimum that lies within the range of the data. From the variational principal, D_{10} and D_{01} must both be identically zero. The ten nonzero parameters obtained from the fit are

TABLE III. Parameters for the generalized two-dimensional cubic function [Eq. (1)] used to fit $E(a, c)$.

D_{30}	-0.518 029 51	D_{03}	-0.000 584 04
D_{21}	0.002 892 93	D_{12}	-0.001 366 44
D_{20}	0.965 682 77	D_{02}	0.002 002 88
D_{11}	-0.000 255 28	D_{00}	-2.612 597 53
a_0	4.625 967 74	c_0	12.818 864 30

listed in Table III. The quality of the fit to the data is exceptional, with a standard deviation of only 27 $\mu\text{Ry}/\text{cell}$ out of a fitted binding energy range of 0.016 Ry/cell, clearly indicating the high level of numerical stability achieved with GTOFF.

The lattice parameters a , c , c/a , and V_0 obtained from the cubic fit [Eq. (1) and Table III] are compared with various theoretical and experimental results in Table IV. The theoretical values include all-electron FLAPW results⁴⁰ and two sets of PP results.^{43,44} The experimental data are comprised of three sets of room-temperature measurements^{4,5,62} and a set of 100 K estimates derived from the room-temperature results of Ref. 4 by applying thermal expansion data for pyrolytic graphite.⁶³ The theoretical values for the intraplanar lattice parameter are all slightly smaller than the experimental 100-K estimate, as is usual for LDA calculations. In contrast, the calculated interplanar lattice parameters all exhibit an anomalous expansion relative to the experimental 100-K estimate, indicating that the LDA potential slightly underestimates the weak van der Waals interaction between the layers. This underbinding can be understood as a manifestation of the well-known inability of the LDA to accurately represent the $1/z$ potential seen by an electron far from a surface, or in this case a graphene layer. The 0.6% contraction in a and 1.6% expansion in c combine to produce a small (0.4%) expansion of the atomic volume.

The analytical form of Eq. (1) can be used to determine a number of additional properties of graphite via elastic theory, as was discussed in detail by Jansen and Freeman.⁴⁰ Three linear combinations of the five independent elastic constants for graphite can be determined from the second derivatives of $E(a, c)$, each associated with a symmetry-preserving distortion of the lattice:

TABLE IV. Comparison of theory and experiment for the zero-pressure lattice parameters (a and c ; bohr), c/a ratio, and cell volume (V_0 ; bohr³/atom) for graphite.

Source	a	c	c/a	V_0
PP (Ref. 43)	4.632	12.70	2.742	58.99
PP (Ref. 44)	4.611	12.622	2.737	58.10
FLAPW (Ref. 40)	4.647	12.903	2.777	60.33
LCGTO-FF (Present)	4.626	12.819	2.771	59.39
Expt. 295 K (Ref. 4)	4.653	12.674	2.724	59.41
Expt. 300 K (Ref. 5)	4.647	12.673	2.726	59.25
Expt. 293 K (Ref. 62)	4.651	12.678	2.726	59.38
Expt. 100 K ^a	4.654	12.619	2.711	59.17

^aValues at 100 K obtained from the room-temperature data of Ref. 4 by applying thermal expansion data for pyrolytic graphite from Ref. 63.

TABLE V. Theoretical and experimental values for four symmetry-preserving elastic constants of graphite; ($C_{11}+C_{12}$), C_{33} , C_{13} , and C' (in Mbar).

Source	$(C_{11}+C_{12})$	C_{33}	C_{13}	C'
FLAPW (Ref. 40)	14.3	0.56	-0.12	2.65
LCGTO-FF (Present)	12.796	0.408	-0.005	2.272
Expt. 300 K (Ref. 8)	12.4	0.365	0.15	2.088
Expt. 0 K (Ref. 12)	13.3	0.41	0.40	2.086

$$C_{11}+C_{12}=\frac{a_0^2}{2V_0}\frac{\delta^2 E}{\delta a^2}, \quad (2)$$

$$C_{33}=\frac{c_0^2}{V_0}\frac{\delta^2 E}{\delta c^2}, \quad (3)$$

$$C_{13}=\frac{c_0 a_0}{2V_0}\frac{\delta^2 E}{\delta a \delta c}. \quad (4)$$

Resolution of C_{11} and C_{12} would require some symmetry-breaking distortion, such as a uniaxial compression perpendicular to the c axis. One additional symmetry-preserving elastic constant that can be derived from those already given is the tetragonal shear modulus,

$$C'=\frac{1}{6}[(C_{11}+C_{12})+2C_{33}-4C_{13}], \quad (5)$$

associated with volume-conserving tetragonal distortions along the c axis.

The four symmetry-preserving elastic constants ($C_{11}+C_{12}$), C_{33} , C_{13} , and C' obtained here are compared with the FLAPW results of Jansen and Freeman⁴⁰ and ultrasound (US) data^{8,12} in Table V. The FLAPW results were obtained from a quadratic fit to 13 energies, whereas the present results were obtained from a cubic fit to 24 energies. For this reason, the LCGTO-FF elastic constants should be more precise than the FLAPW results. The LCGTO-FF predictions for $(C_{11}+C_{12})$ and C_{33} differ from the 0 K values of Gauster and Fritz¹² by less than 5%. This level of agreement is quite good for parameters that are determined from second derivatives of a fitted curve. There is however a serious disagreement between the measured values of C_{13} and the theoretical results, with the former being positive and the latter being negative. (Both theoretical values are zero within the limits of precision for the respective calculations.⁴⁰) This discrepancy will be discussed further below.

The symmetry-preserving elastic constants given in Table V can be used to generate other parameters that are routinely accessible with hydrostatic EOS measurements, thereby providing an independent test for the quality of the present results. As was discussed by Jansen and Freeman,⁴⁰ the static-lattice bulk modulus B can be calculated from

$$B=\frac{C_{33}(C_{11}+C_{12})-2C_{13}^2}{(C_{11}+C_{12})+2C_{33}-4C_{13}} \quad (6)$$

while the pressure derivatives of the hexagonal lattice constants are given by

TABLE VI. Theoretical and experimental values for the bulk modulus (B ; Mbar) and pressure derivatives of the lattice parameters (a' and c' ; Mbar $^{-1}$) for graphite. (Present values are from a cubic fit. US, ultrasound data; EOS, equation of state data.)

Source	B	a'	c'
FLAPW (Ref. 40)	0.502	-0.0852	-1.82
LCGTO-FF (Present)	0.383	-0.0791	-2.45
EOS 300 K (Ref. 5)	0.338	-0.0800	-2.80
US 300 K (Ref. 8)	0.358	-0.0480	-2.70
US 0 (Ref. 12)	0.410	-0.0019	-2.44

$$a' \equiv \frac{\delta}{\delta P} \left(\frac{a}{a_0} \right) = \frac{C_{33} - C_{13}}{2C_{13}^2 - C_{33}(C_{11} + C_{12})} \quad (7)$$

and

$$c' \equiv \frac{\delta}{\delta P} \left(\frac{c}{c_0} \right) = \frac{(C_{11} + C_{12}) - 2C_{13}}{2C_{13}^2 - C_{33}(C_{11} + C_{12})}. \quad (8)$$

The values obtained here for these parameters are listed in Table VI along with results from the FLAPW calculations,⁴⁰ values deduced from the US elastic constant data in Table V,^{8,12} and values obtained directly from hydrostatic EOS data.⁵ For B and c' there is good consistency between the experimental data and the present LCGTO-FF results, with the room-temperature values of $B(c')$ being smaller (larger) than the 0 K values, as would be expected on physical grounds. There is, however, a significant discrepancy between the US and EOS values of a' , with the latter value being in good agreement with both theoretical results. The disagreement between the US and LCGTO-FF values for a' is clearly due to using different values for C_{13} ; see Table V. Thus, the fact that the present result for a' is in good agreement with the EOS measurements provides powerful indirect evidence that the LCGTO-FF result for C_{13} is more reliable than the US measurement.

V. EOS AND HIGH-PRESSURE PROPERTIES

Since c' is more than an order of magnitude larger than a' , the anisotropy of graphite will decrease rapidly under pressure. For this reason, the asymmetrical reference orbital basis set used thus far is not suitable for calculating the high-pressure EOS of graphite. At the same time, any attempt to use two different basis sets to calculate the low- and high-pressure portions of the EOS will inevitably produce a discontinuity in the binding energy curve. To avoid these difficulties, the entire EOS of graphite was calculated using a symmetrical orbital basis set, formed by removing the one extra p_z GTO from the reference basis. Although this change in the basis set will produce a slight reduction in the precision of the calculations, the impact of the change will be largest at zero pressure, where it can be assessed by comparison with the results obtained with the reference basis set, and then get progressively smaller as the system becomes more symmetrical under pressure.

Nine equally spaced cell volumes ranging between 0.7 and 1.1 times the zero-pressure volume from the cubic fit were chosen for consideration. Electronic structure calcula-

tions were then carried out at four or five evenly spaced values of c/a for each volume; i.e., the crystal was subjected to a volume conserving tetragonal distortion. A total of 43 binding energies were generated in this manner.⁶⁴

Although the two-dimensional cubic function given in Eq. (1) provides an excellent fit to the binding energy of graphite near the energy minimum, it cannot be expected to fit energies that are far from the minimum. For this reason, an alternative approach was used to extract the EOS of graphite from the 43 binding energies. First, the binding energies for each volume were fitted with a third-order function of a to determine the minimum energy and c/a ratio for that volume. The cubic fit parameters were also used to calculate the tetragonal shear modulus at each volume using the equation

$$C^t = \frac{a_0^2}{12V_0} \left[\frac{\delta^2 E}{\delta a^2} \right]_V. \quad (9)$$

The energies of the two optical transitions near the K point, A_1 and A_2 ,⁶ were also estimated for each volume via a linear interpolation. The binding energies, c/a ratios, shear moduli, and optical transition energies determined in this fashion are listed in Table VII. A detailed comparison of the symmetrical orbital basis set results for $V = V_0$ with the reference basis set results reveals that the reduced basis set size produces a 3 mRy increase in the binding energy, a 0.14% reduction in c/a , an 8% increase in C^t , and a 0.04 eV increase (decrease) in $A_1(A_2)$.

To allow a more precise determination of the EOS for graphite, binding energies were calculated for three additional cell volumes near the energy minimum using a single interpolated c/a value for each volume, see Table VII. The static-lattice EOS was then determined by fitting all 12 binding energies in Table VII with a third-order polynomial in $V^{-1/3}$. The fitted binding curve is compared with the calculated binding energies in Fig. 2. The standard deviation for the fit was only 0.33 mRy/cell out of a total energy range of 73.80 mRy/cell. Pressures obtained from the EOS fit for the 12 volumes used here are given in Table VII.

The zero-pressure cell volumes, binding energies, and bulk moduli (B_0) obtained with the EOS fit and the earlier cubic fit are compared with other LDA calculations^{40,43,44} and hydrostatic data^{4,5,62} in Table VIII. (The zero-pressure c/a value listed for the EOS fit was obtained from a linear interpolation.) The equilibrium cell volume determined with the EOS fit is 1.6% smaller than that obtained with the more precise cubic fit. In similar work on corundum,⁶⁵ using a single basis set, it was found that the cell volumes obtained from cubic and EOS fits differed by less than 4 parts per million. This suggests that the much larger volume shift found for graphite is largely due to the change in the basis set, not the difference between the two fitting procedures. The reduction in volume then causes a slight decrease in c/a and a significant (33%) increase in B_0 . In spite of these shifts, the zero-pressure results from the EOS fit are generally consistent with the results of prior calculations and are in acceptable agreement with the experimental data, given the exceptional softness of graphite.

The pressure versus volume curve obtained from the EOS fit is compared with room-temperature data^{4,5} in Fig. 3. The data of Zhao and Spain⁴ (ZS) show considerable scatter,

TABLE VII. Binding energy (E_b ; Ry/cell), c/a ratio, tetragonal shear modulus (C^t ; Mbar), optical transition energies (A_1 and A_2 ; eV), and fitted pressure (P ; GPa) for each fractional volume (V/V_0 ; $V_0 = 237.5666 \text{ bohr}^3$).

V/V_0	E_b	c/a	C^t	A_1	A_2	P
1.10	-2.605 443	3.023 6	2.173	0.38	0.39	-4.06
1.05	-2.607 912	2.894 1	2.033	0.50	0.52	-2.73
1.025	-2.608 754	2.83 ^a	-1.86
1.00	-2.609 491	2.767 1	2.452	0.66	0.69	-0.80
0.975	-2.609 510	2.70 ^a	0.45
0.95	-2.609 126	2.643 1	2.446	0.84	0.90	1.96
0.925	-2.608 076	2.58 ^a	3.75
0.90	-2.605 889	2.519 5	2.628	1.06	1.21	5.89
0.85	-2.599 930	2.403 8	2.944	1.32	1.59	11.47
0.80	-2.586 117	2.288 0	3.393	1.64	2.08	19.44
0.75	-2.566 973	2.183 9	3.815	2.01	2.67	30.84
0.70	-2.535 710	2.090 3	4.563	2.44	3.37	47.35

^aInterpolated c/a values.

suggesting that it may have been taken under nonhydrostatic conditions, thereby providing an upper bound to the room-temperature hydrostat. Since the data of Hanfland *et al.*⁵ is smoother and lies along the lower edge of the ZS data, it probably gives a better representation of the 300-K isotherm. On the other hand, the theoretical curve in Fig. 2 models the 0-K isotherm and should therefore act as a lower bound to the room-temperature hydrostat. Instead, the calculated curve provides a rather good fit to the 300-K data of Hanfland *et al.*⁵ with the exception of passing well below the measured zero-pressure point. This result suggests that the present LDA calculations slightly overestimate the volume at each pressure. This result is consistent with the earlier suggestion that the LDA model underestimates the weak van der Waals interplanar binding. Overall, the present calculations agree with the experimental data to the extent that can be expected for state-of-the-art LDA calculations such as these.

Graphite Binding Curve

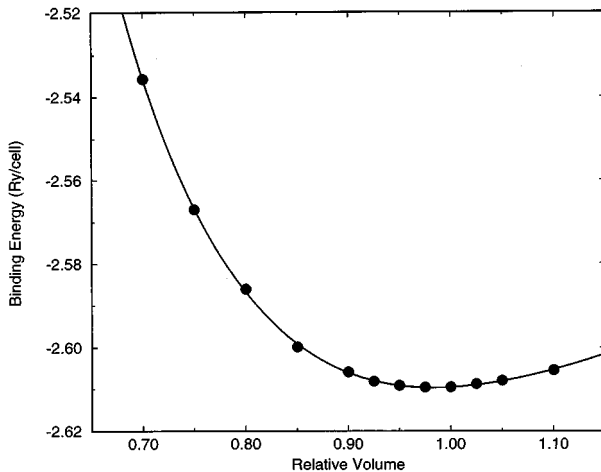


FIG. 2. Calculated binding energies (Ry/cell) and fitted binding curve for graphite, relative to the zero-pressure volume found with the cubic fit; $V_0 = 237.5666 \text{ bohr}^3$.

The calculated c/a values listed in Table VII are plotted as a function of relative volume in Fig. 4, along with the 300-K data of ZS (Ref. 4) and FLMTO results taken from Table I of Ahuja *et al.*⁴⁵ (The c/a values given in Table I of Ref. 45 do not agree with the values plotted in Fig. 6 of that reference. This inconsistency is not fully understood at this time.⁶⁰) The c/a values obtained here form a smooth line that lies slightly above the experimental data and steadily converges with that data as the volume is reduced. This result can be understood as another manifestation of the LDA underestimate of the weak van der Waals interlayer bonding. When the volume is reduced under pressure, the anisotropy of the bonding is also reduced, as is evidenced by the smaller c/a ratio and larger tetragonal shear modulus. Thus, the LDA potential is better able to model the interlayer bonding at high pressures. For $V \approx V_0$, the FLMTO result in Fig. 4 is in nearly perfect agreement with the LCGTO-FF result. As the volume is decreased, however, the FLMTO curve crosses the experimental data and then runs roughly parallel with the

TABLE VIII. Zero-pressure values for the volume (V_0 ; $\text{bohr}^3/\text{cell}$), c/a ratio, binding energy (E_0 ; Ry/cell), and bulk modulus (B_0 ; Mbar) obtained from the third-order EOS fit are compared with previous electronic structure results and hydrostatic data.

Source	V_0	c/a	E_0	B_0
PP (Ref. 43)	235.98	2.742	-2.59	...
PP (Ref. 44)	232.407	2.737	-2.654	...
FLAPW (Ref. 40)	241.305	2.777	...	0.502
LCGTO-FF (EOS fit)	233.651	2.726	-2.610	0.509
LCGTO-FF (cubic fit)	237.567	2.771	-2.613	0.383
Expt. 295 K (Ref. 4)	237.64	2.724	...	0.308
Expt. 300 K (Ref. 5)	237.00	2.726	...	0.338
Expt. 293 K (Ref. 62)	237.51	2.726
Expt. 100 K ^a	236.71	2.711

^aValues at 100 K obtained from the room-temperature data of Ref. 4 by applying thermal expansion data for pyrolytic graphite from Ref. 63.

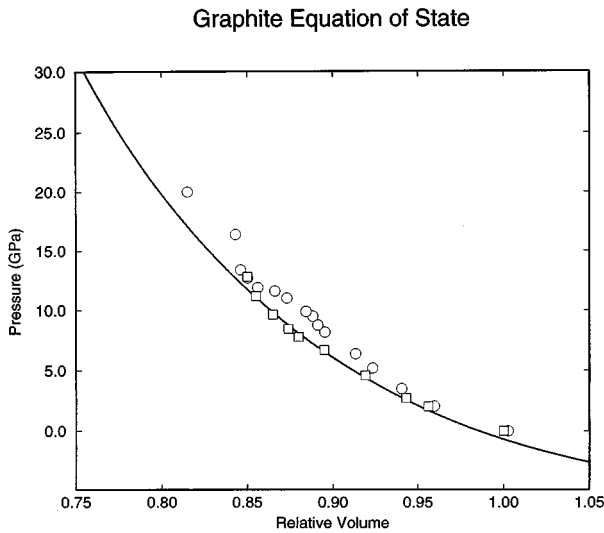


FIG. 3. Calculated pressure vs relative volume curve compared with room-temperature data from Ref. 4 (circle) and Ref. 5 (square). The reference volume is the ambient volume from Ref. 5; $V_0 = 237.00 \text{ bohr}^3$.

data. In general, the behavior of the LCGTO-FF c/a curve seems more plausible than the behavior of the FLMTO curve.

The optical transition energies A_1 and A_2 are plotted as functions of pressure in Fig. 5, along with 300-K reflectivity data from Hanfland *et al.*⁶ and FLMTO results from Ahuja *et al.*⁴⁵ For A_1 , the LCGTO-FF curve is in excellent agreement with the experimental data, whereas the FLMTO curve lies about 0.1 eV below the data. Roughly one-third of the difference between the LCGTO-FF and FLMTO results (0.04 eV) can be attributed to the use of the symmetrical

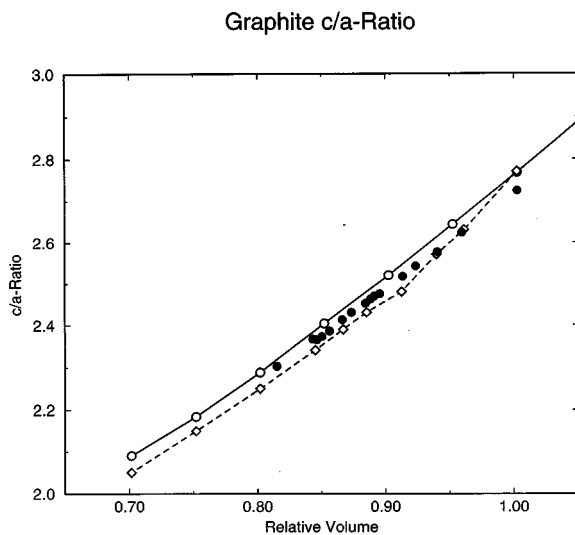


FIG. 4. The c/a ratio vs relative volume curve from the present LCGTO-FF calculations (solid line) is compared with the FLMTO results of Ref. 45 (dashed line) and room-temperature data from Ref. 4 (solid circles). The reference volume is the ambient volume from Ref. 5; $V_0 = 237.00 \text{ bohr}^3$.

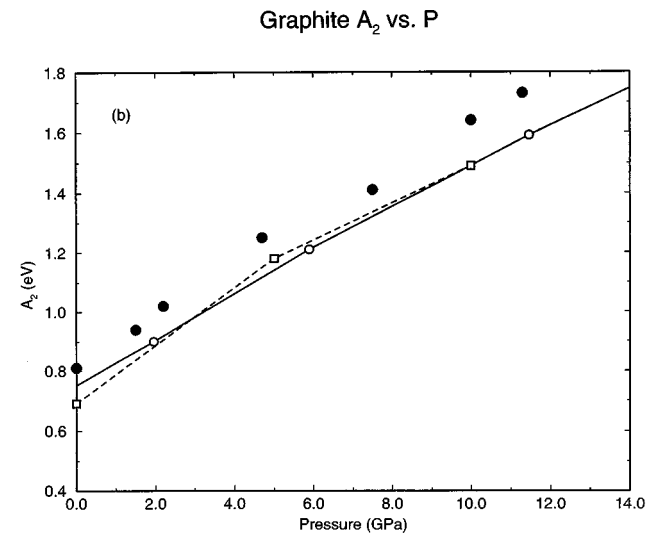
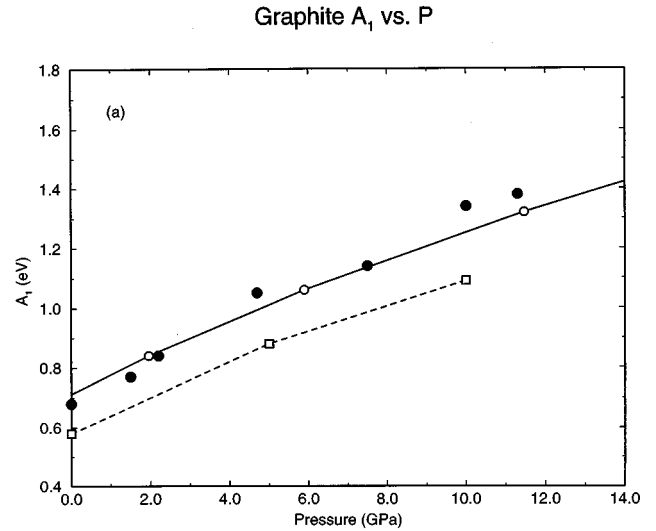


FIG. 5. The optical transition energies A_1 (a) and A_2 (b) are shown as functions of pressure for the present LCGTO-FF calculations (solid line), the FLMTO calculations of Ref. 45 (dashed line), and the room-temperature measurements of Ref. 6 (solid circles).

orbital basis set instead of the larger reference basis set. The remaining difference between the two calculations probably is not significant. For A_2 , the LCGTO-FF and FLMTO curves are in good agreement, with both lying 0.1–0.2 eV below the experimental curve. Both LDA calculations accurately reproduce the pressure dependence of the optical transitions.

VI. CONCLUSIONS

The all-electron, full-potential LCGTO-FF technique has been used to perform high-precision electronic structure calculations on bulk graphite. An analysis of the zero-pressure electronic structure indicates that the large inconsistencies between the PP band-structure calculations^{41,43,44} and prior all-electron calculations^{40,45} were, in fact, due to inaccuracies in the all-electron calculations. The present all-electron band structure for graphite is consistent with experimental data to the extent that can be expected given the well-known limita-

tions of LDA one-electron energies.

A two-dimensional cubic fit to 24 binding energies calculated for hexagonal lattice parameters near the equilibrium was used to determine zero-pressure values for the lattice parameters and symmetry preserving elastic constants. The intralayer lattice constant found here exhibits the usual LDA-induced contraction, whereas the interlayer separation and the unit-cell volume exhibit an anomalous expansion due to a LDA underestimate of the weak van der Waals interlayer bonding. The calculated values of $C_{11} + C_{12}$ and C_{33} are in good agreement with ultrasound measurements, while the predicted value of C_{13} (≈ 0) is much smaller than the ultrasound value. The bulk modulus and pressure derivatives of the lattice constants derived from the theoretical elastic constants are in excellent agreement with diamond anvil cell (DAC) data, suggesting that the theoretical result for C_{13} is probably more reliable than the ultrasound measurement.

A second set of LCGTO-FF calculations was used to generate an analytical EOS for graphite for pressures up to 50 GPa, well beyond the stability range for the graphite structure. The fitted EOS and the pressure dependencies of the c/a ratio and optical transition energies (A_1 and A_2) are in good agreement with DAC data up to 14 GPa. Many of the trends in the calculated results again suggest that the LDA potential slightly underestimates the weak van der Waals interlayer bonding. As the volume is reduced under pressure, the anisotropy in the bonding is also reduced and the LDA results become more reliable.

ACKNOWLEDGMENTS

Helpful communications with J. M. Wills, S. B. Trickey, B. I. Dunlap, and M. C. Schabel are acknowledged. This work was supported by the U.S. Department of Energy.

-
- ¹For a review of early work on graphite, see B. T. Kelly, *Physics of Graphite* (Applied Science, London, 1981).
- ²R. Clarke and C. Uher, *Adv. Phys.* **33**, 469 (1984).
- ³B. Alzyab, C. H. Perry, C. Zahopoulos, O. A. Pringle, and R. M. Nicklow, *Phys. Rev. B* **38**, 1544 (1988).
- ⁴Y. X. Zhao and I. L. Spain, *Phys. Rev. B* **40**, 993 (1989).
- ⁵M. Hanfland, H. Beister, and K. Syassen, *Phys. Rev. B* **39**, 12 598 (1989).
- ⁶M. Hanfland, K. Syassen, and R. Sonnenschein, *Phys. Rev. B* **39**, 12 598 (1989).
- ⁷T. Yagi, W. Utsumi, M. Yamakata, T. Kikegawa, and O. Shimomura, *Phys. Rev. B* **46**, 6031 (1992).
- ⁸O. L. Blaklee, D. G. Proctor, E. J. Seldin, G. B. Spence, and T. Weng, *J. Appl. Phys.* **41**, 3373 (1970).
- ⁹G. B. Spence and E. J. Seldin, *J. Appl. Phys.* **41**, 3383 (1970); also, E. J. Seldin and C. W. Nezbeda, *ibid.* **41**, 3389 (1970).
- ¹⁰F. Tuinstra and J. L. Koenig, *J. Chem. Phys.* **53**, 1126 (1970).
- ¹¹R. Nicklow, N. Wakabayashi, and H. G. Smith, *Phys. Rev. B* **5**, 4951 (1972).
- ¹²W. B. Gauster and J. J. Fritz, *J. Appl. Phys.* **45**, 3309 (1974).
- ¹³R. F. Willis, B. Feuerbacher, and B. Fitton, *Phys. Lett.* **34A**, 231 (1971).
- ¹⁴G. Bellodi, A. Borghesi, G. Guizzetti, L. Nosenzo, E. Reguzzoni, and G. Samoggia, *Phys. Rev. B* **12**, 5951 (1975).
- ¹⁵M. S. Dresselhaus and G. Dresselhaus, *Phys. Rev. B* **13**, 4635 (1976).
- ¹⁶P. M. Williams, *Nuovo Cimento B* **38**, 216 (1977).
- ¹⁷A. Bianconi, S. B. M. Hagstrom, and R. Z. Bachrach, *Phys. Rev. B* **16**, 5543 (1977).
- ¹⁸W. Eberhardt, L. T. McGovern, E. W. Plummer, and J. E. Fisher, *Phys. Rev. Lett.* **44**, 200 (1980).
- ¹⁹V. Dose, G. Reusing, and H. Scheidt, *Phys. Rev. B* **26**, 984 (1982).
- ²⁰C. F. Hague, G. Indlekofer, U. M. Gubler, V. Geiser, P. Oelhafen, H. J. Güntherodt, J. Schmidt-May, R. Nyholm, E. Wuilloud, and Y. Baer, *Synth. Met.* **8**, 131 (1983).
- ²¹Th. Fauster, F. J. Himpsel, J. E. Fischer, and E. W. Plummer, *Phys. Rev. Lett.* **51**, 430 (1983).
- ²²A. R. Law, J. J. Barry, and H. P. Hughes, *Phys. Rev. B* **28**, 5332 (1983).
- ²³D. Marchand, C. Fretigny, M. Lagues, F. Batallan, C. Simon, I. Rosenman, and R. Pinchaux, *Phys. Rev. B* **30**, 4788 (1984).
- ²⁴T. Takahashi, H. Tokailin, and T. Sagawa, *Solid State Commun.* **52**, 765 (1984).
- ²⁵A. R. Law, M. T. Johnson, H. P. Hughes, and H. A. Padmore, *J. Phys. C* **18**, L297 (1985).
- ²⁶T. Takahashi, H. Tokailin, and T. Sagawa, *Phys. Rev. B* **32**, 8317 (1985).
- ²⁷B. Reihl, J. K. Gimzewski, J. M. Nicholls, and E. Tosatti, *Phys. Rev. B* **33**, 5770 (1986).
- ²⁸Schäfer, M. Schlüter, and M. Skibowski, *Phys. Rev. B* **35**, 7663 (1987).
- ²⁹F. Maeda, T. Takahashi, H. Ohsawa, S. Suzuki, and H. Suematsu, *Phys. Rev. B* **37**, 4482 (1988).
- ³⁰W. Schülke, U. Bonse, H. Nagasawa, A. Kaprolat, and A. Berthold, *Phys. Rev. B* **38**, 2112 (1988).
- ³¹R. Claessen, H. Cartensen, and M. Skibowski, *Phys. Rev. B* **38**, 12 582 (1988).
- ³²I. R. Collins, P. T. Andrews, and A. R. Law, *Phys. Rev. B* **38**, 13 348 (1988).
- ³³D. A. Fischer, R. M. Wentzcovitch, R. G. Carr, A. Continenza, and A. J. Freeman, *Phys. Rev. B* **44**, 1427 (1991).
- ³⁴For a review of early electronic structure calculations on graphite see R. C. Tatar and S. Rabii, *Phys. Rev. B* **25**, 4126 (1982).
- ³⁵M. Weinert, E. Wimmer, and A. J. Freeman, *Phys. Rev. B* **26**, 4571 (1982).
- ³⁶N. A. W. Holzwarth, S. G. Louie, and S. Rabii, *Phys. Rev. B* **26**, 5382 (1982).
- ³⁷D. P. DiVincenzo, E. J. Mele, and N. A. W. Holzwarth, *Phys. Rev. B* **27**, 2458 (1983).
- ³⁸M. Posternak, A. Baldereschi, A. J. Freeman, and E. Wimmer, *Phys. Rev. Lett.* **52**, 863 (1984); also M. Posternak, A. Baldereschi, A. J. Freeman, E. Wimmer, and M. Weinert, *ibid.* **50**, 761 (1983).
- ³⁹M. T. Yin and M. L. Cohen, *Phys. Rev. B* **29**, 6996 (1984); S. Fahy, S. G. Louie, and M. L. Cohen, *ibid.* **35**, 7623 (1987).
- ⁴⁰H. J. F. Jansen and A. J. Freeman, *Phys. Rev. B* **35**, 8207 (1987).
- ⁴¹J. C. Charlier, X. Gonze, and J. P. Michenaud, *Phys. Rev. B* **43**, 4579 (1991).
- ⁴²S. B. Trickey, F. Müller-Plathe, G. H. F. Diercksen, and J. C.

- Boettger, Phys. Rev. B **45**, 4460 (1992); S. B. Trickey, G. H. F. Diercksen, and F. Müller-Plathe, Astrophys. J. **336**, L37 (1989).
- ⁴³M. C. Schabel and J. L. Martins, Phys. Rev. B **46**, 7185 (1992).
- ⁴⁴J. Furthmüller, J. Hafner, and G. Kresse, Phys. Rev. B **50**, 15 606 (1994).
- ⁴⁵R. Ahuja, S. Auluck, J. Trygg, J. M. Wills, O. Eriksson, and B. Johansson, Phys. Rev. B **51**, 4813 (1995).
- ⁴⁶J. D. Bernal, Proc. R. Soc. London, Ser. A **106**, 749 (1924); for a detailed description of this structure, with diagrams, see Ref. 34.
- ⁴⁷J. C. Boettger, Int. J. Quantum Chem. Symp. **29**, 197 (1995).
- ⁴⁸J. C. Boettger, Int. J. Quantum Chem. Symp. **27**, 147 (1993); also see, J. C. Boettger and S. B. Trickey, Phys. Rev. B **32**, 1356 (1985); J. W. Mintmire, J. R. Sabin, and S. B. Trickey, *ibid.* **26**, 1743 (1982).
- ⁴⁹U. Birkenheuer, J. C. Boettger, and N. Rösch, J. Chem. Phys. **100**, 6826 (1994); U. Birkenheuer, Ph.D. dissertation, TU München, 1994.
- ⁵⁰L. Hedin and B. I. Lundqvist, J. Phys. C **4**, 2064 (1971).
- ⁵¹B. I. Dunlap, J. W. D. Connolly, and J. R. Sabin, J. Chem. Phys. **71**, 3396 (1979).
- ⁵²J. C. Boettger, Int. J. Quantum Chem. Symp. **30**, 133 (1996).
- ⁵³J. A. Appelbaum and D. R. Hamann, Solid State Commun. **27**, 881 (1978).
- ⁵⁴C. S. Wang and A. J. Freeman, Phys. Rev. B **21**, 4585 (1980).
- ⁵⁵K. Mednick and L. Kleinman, Phys. Rev. B **22**, 5768 (1980).
- ⁵⁶B. I. Dunlap and J. C. Boettger, J. Phys. B **29**, 4907 (1996).
- ⁵⁷P. E. Blöchl, O. Jepsen, and O. K. Andersen, Phys. Rev. B **49**, 16 223 (1994).
- ⁵⁸J. C. Slonczewski and P. R. Weiss, Phys. Rev. **109**, 272 (1958).
- ⁵⁹J. Perdew and A. Zunger, Phys. Rev. B **23**, 5048 (1981).
- ⁶⁰J. M. Wills (private communication).
- ⁶¹J. M. Wills and O. Eriksson, Phys. Rev. B **45**, 13 879 (1992).
- ⁶²J. Donohue, *The Structures of the Elements* (Kreiger, Malabar, 1982), p. 256.
- ⁶³*Thermophysical Properties of Matter*, edited by Y. S. Touloukian, R. K. Kirby, R. E. Taylor, and T. Y. R. Lee (Plenum, New York, 1977), Vol. 13, p. 79.
- ⁶⁴The 43 calculated values of E_b for graphite are available on request from the author.
- ⁶⁵J. C. Boettger, Phys. Rev. B **55**, 750 (1997).